AIAA JOURNAL
Vol. 35, No. 4, April 1997

New Methodology for the Measurement of Surface Shear Stress Vector Distributions

Daniel C. Reda,* Michael C. Wilder,† Dino J. Farina,‡ and Greg Zilliac§
NASA Ames Research Center, Moffett Field, California 94035-1000

When a liquid crystal coating (LCC) is illuminated from the normal direction by white light and observed from an oblique above-plane view angle, its color-change response to shear depends on both shear stress vector magnitude and the direction of the applied shear vector relative to the observer's in-plane line of sight. At any point, the maximum color change is always measured when the local shear vector is aligned with, and directed away from, the observer; the magnitude of the color change at this vector/observer aligned orientation scales directly with shear stress magnitude. Based on this knowledge, a full-surface shear stress vector measurement methodology was formulated. An image-based system, incorporating a three-chip color video camera, linked to a frame grabber and computer, was devised to test the method. Full-surface images of LCC color-change response to a three-dimensional turbulent wall jet flowing over a planar surface were acquired and analyzed to define the surface shear stress vector field. Comparisons of these first-ever such results to conventional point measurements, obtained via the oil-drop interferometry technique, yielded very good agreement, corroborating the new method. Based on present results, it has been shown that the liquid crystal coating technique can be utilized to obtain areal measurements of surface shear stress vector distributions on planar surfaces with accuracies equivalent to conventional point-measurement techniques.

Nomenclature

D	= jet exit diameter
P_0	= wall jet stagnation pressure on the exit plane centerline
V	= velocity
x	= axial coordinate on test surface measured from jet exit plane
y	= transverse coordinate on test surface measured from jet centerline
α	= above-plane view angle, measured positive upward from zero in plane of test surface
$\Delta\phi$	= spacing between adjacent ϕ angles
σ	= standard deviation
τ	= magnitude of surface shear stress vector
$\bar{\tau}$	= average shear stress vector magnitude
$\vec{\tau}$	= shear stress vector
ϕ	= circumferential angle in plane of test surface, measured positive counterclockwise from origin at jet centerline
ϕ_τ	= orientation of surface shear stress vector directed away from observer with an in-plane line of sight at $\phi = \phi_\tau$
$\bar{\phi}_\tau$	= average shear stress vector orientation

Subscripts

C	= camera
J	= jet
L	= light

I. Introduction

THE objective of this continuing research is to develop an image-based instrumentation system for the areal visualization and measurement of the instantaneous shear stress vector distribution acting on any aerodynamic configuration. In the near term, the impact of such a measurement technique would be to provide modelers with detailed data sets for code-validation purposes. The availability of continuous surface shear stress vector distributions measured in fundamental (building-block-type) experiments, especially those involving three-dimensional boundary layers, separation, and/or reattachment, would be of great benefit to the development of advanced, viscous-flow computational tools. In the long term, the application of such a full-surface visualization/measurement methodology to aerodynamic testing would significantly improve the productivity of ground-based facilities. The creation of advanced design codes, coupled with an increased productivity of large-scale wind tunnels, would ultimately result in reduced design-cycle times and increased performance for new commercial and military aviation products.

The approach has been to systematically explore the color-change responses of shear-stress-sensitive, temperature-insensitive liquid crystal coatings (LCC) to applied shear stresses of known magnitudes and known directions relative to the observer.[1,2]

The liquid crystal phase of matter is a weakly ordered, viscous, fluidlike state that exists between the nonuniform liquid phase and the ordered solid phase of certain organic compounds.[3] Liquid crystals can exhibit optical properties that are characteristic of solid, crystalline materials. If a thin film of liquid crystals is applied to a solid surface and the molecules within the coating are aligned by frictional forces into the required planar state, then this molecular structure selectively scatters incident white light as a three-dimensional spectrum or color space.

It has been known for some time that changes in applied shear stress magnitude cause the liquid crystal molecular structure to change, reorienting the scattered light spectrum in space.[4] A fixed observer thus sees a color change in response to the altered shearing force. Such color changes are continuous and reversible, with time response on the order of milliseconds. Based on these characteristics, LCC have been used to obtain qualitative areal visualizations of shear stress magnitudes acting on aerodynamic surfaces in both wind-tunnel[5] and flight-test[6] applications.

Recently, Reda and Muratore[2] showed that LCC color-change response to shear depends on both shear stress magnitude and the direction of the applied shear relative to the observer's line of sight. Under normal white light illumination and for oblique observation, liquid crystal color-change responses were quantified by subjecting a planar coating to a wall-jet shear flow; scattered light spectra were measured at a point on the wall-jet centerline using a fiber-optic

Presented as Paper 96-0420 at the AIAA 34th Aerospace Sciences Meeting, Reno, NV, Jan. 15–18, 1996; received July 22, 1996; revision received Dec. 20, 1996; accepted for publication Dec. 23, 1996.

*Senior Research Scientist, Fluid Mechanics Laboratory Branch. Associate Fellow AIAA.
†Senior Research Scientist, MCAT Inc. Member AIAA.
‡Graduate Student Researcher, Fluid Mechanics Laboratory Branch; currently President, Image Therm Engineering, Inc., 159 Summer Street, Suite 2R, Waltham, MA 02154.
§Research Scientist, Fluid Mechanics Laboratory Branch.

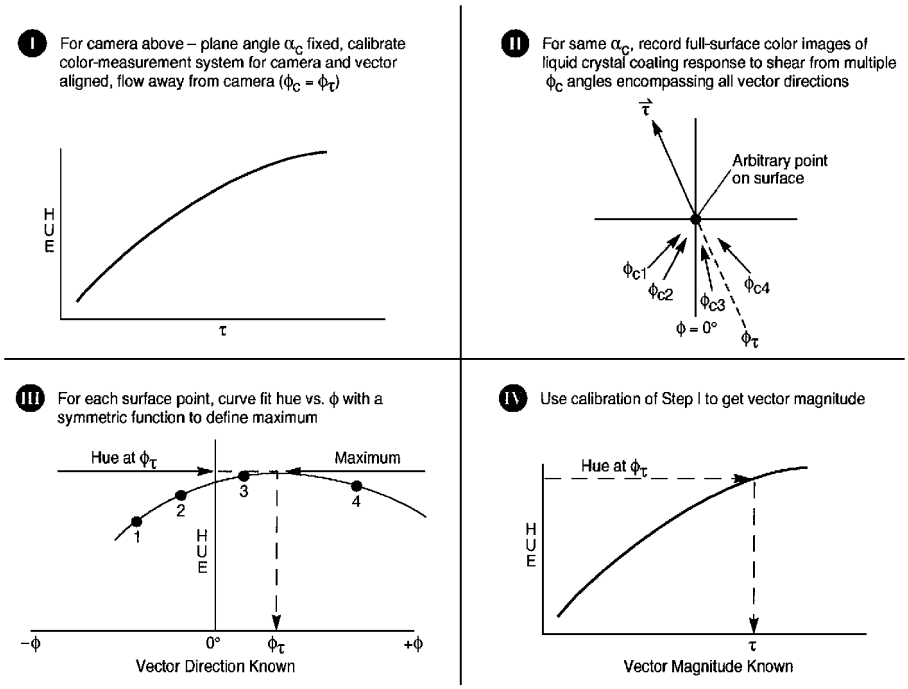

Fig. 1 Shear stress vector measurement methodology.

probe and a spectrophotometer. At any fixed shear stress magnitude, the maximum color change was always measured when the shear vector was aligned with and directed away from the observer; measured color change decreased symmetrically in a Gaussian fashion with changes in the relative in-plane view angle to either side of this vector/observer aligned position. For this vector/observer aligned orientation, color change was found to continually increase with increasing shear stress magnitude over the eightfold range examined. Based on these point-measurement results, a full-surface shear stress vector measurement methodology was formulated; the four-step procedure is summarized in Fig. 1. Figure 2 serves to illustrate the geometry referred to in the description of Fig. 1 given later.

For full-surface measurements, a three-chip red-green-blue (RGB) color video camera, a frame grabber, and a supporting computer are utilized. The coated surface is illuminated from the normal direction ($\alpha_L = 90$ deg), and the camera is positioned at a constant above-plane view angle of $\alpha_C \sim 30$ deg. In step 1, a single calibration curve of color (hue) vs shear magnitude is obtained for the specific arrangement wherein the calibration shear vector is aligned with, and directed away from, the camera. Conventional point-measurement techniques for shear magnitude can be employed for this purpose.[7,8] In step 2, full-surface images of the LCC color-change response to an unknown shear field are recorded from multiple in-plane view angles (here, ϕ_{C1}–ϕ_{C4}) encompassing the vector directions to be measured. In step 3, for each physical point on the test surface, a Gaussian curve is fit to the hue vs in-plane view angle data. The in-plane view angle corresponding to the maximum of the curvefit determines the vector orientation (ϕ_τ). In step 4, the hue value corresponding to the vector orientation is used along with the calibration curve of step 1 to define the vector magnitude (τ). Steps 3 and 4 are repeated for all surface points to determine the complete shear vector field.

In the present research, this new measurement methodology was applied to a turbulent wall-jet flow, yielding, to the authors' knowledge, the first-ever, full-surface shear stress vector measurements. As will be shown, these results compared favorably with point measurements obtained using the established oil-drop interferometry technique.[8]

U.S. patents for the full-surface visualization of reverse-flow regions[9] and for the full-surface measurement of shear stress vector distributions[10] were issued to NASA in 1995, and this technology is available for transfer. Reference 11 provides a demonstration of the newly discovered, expanded flow visualization capabilities of the LCC technique for simultaneous, full-surface observations of both transition and separation.

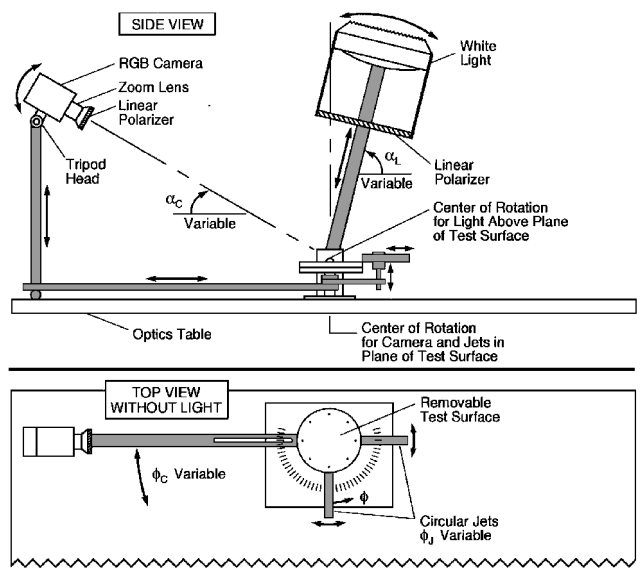

Fig. 2 Schematic of experimental arrangement.

II. Experimental Arrangement and Procedures

A schematic of the experimental arrangement is shown in Fig. 2. The primary feature of this apparatus is that all of its components (the two jets, the light, and the camera) can be independently rotated about the center of the test surface.

The removable test surface was a 6-in.-diam aluminum disk, anodized flat black, with reference marks machined every 45 deg around the circumference. A new LCC was applied to this surface by spray-painting techniques prior to the acquisition of each ϕ_C image; coating uniformity and repeatability issues were addressed in Ref. 2. Hallcrest BCN/192 shear-stress-sensitive liquid crystal compound was used for the measurements. The coatings were illuminated by a 5600 K white light source directed normal to the test surface; the spectrum for this light source was reported in Ref. 2.

Linear polarizers were positioned between the light and the test surface and between the test surface and the color camera; the

relative orientation of these filters was adjusted to minimize reflected glare. The circularly polarized light scattered from the liquid crystal coating was effectively unaltered by this approach.

Only one of the two jets was used in the present experiments. The jet was fed with filtered, dry, room temperature air from a pressurized plenum connected to a compressor. The jet flow issued to atmospheric pressure from a circular steel tube of outer diameter = 0.50 in. and inner diameter = 0.33 in. with a beveled, sharp-edged tip. A notch machined in the beveled wall just upstream of the exit plane allowed for the accurate realignment of the jet exit and the disk edge before each experiment. The longitudinal axis of the jet tube was always parallel to the test surface, and this axis was aligned with the $\phi = 0$ deg reference to within ± 1 deg.

Pressure control and repeatability were achieved by utilizing an electropneumatic proportional/integral/derivative controller linked to a high-flow-capacity pressure regulator. The desired total pressure at the exit plane of the jet ($0.5 \leq P_0 \leq 5.0$ psig) was input to the controller from the lab computer. System feedback was provided by a miniature pitot probe of tip diameter 0.031 in. that entered the stream from above, through the outer half of the jet flow. The probe stagnation pressure was input to a high-accuracy differential pressure transducer, referenced to atmospheric pressure, and the resulting output signal provided feedback to the controller. Jet centerline total pressure at the exit could thus be maintained constant with a standard deviation of less than or equal to 1% of the setpoint value over the stated range. Corresponding jet centerline exit velocities were in the range $250 \leq V_J \leq 790$ ft/s.

Fluctuations in the surface shear stress magnitude were measured on the wall-jet centerline at the center of the test surface using a glue-on hot-film sensor (DANTEC probe type 55) linked to a constant temperature anemometer. This sensor was calibrated against the oil-drop technique[8] (to be discussed in a subsequent section). At $P_0 = 4$ psig, the hot-film data, sampled at both 30 Hz (the camera sampling rate) and 1 kHz, yielded a normal probability density function with a standard deviation of 15%; i.e., significant fluctuations in the instantaneous surface shear stress magnitude were found to be present within the core region of this flow. The influence of such fluctuations on the measured LCC color-change responses will be discussed later in this section.

The surface streakline pattern produced by this wall-jet flow with a jet exit pressure of $P_0 = 4$ psig is shown in Fig. 3. This pattern was the result of an oil-flow visualization experiment conducted using a very low viscosity LCC (EM Industries TI511). Note that the higher viscosity liquid crystals utilized to obtain the color-change/shear-field measurements did not flow; selection of LCC mixtures is discussed in Ref. 2. The oil-flow streaks are generally assumed to be tangent to the local shear stress vector at every point along a given streak trajectory. Shear vector directions measured from this pattern are later compared with shear vector directions determined by the measurement methodology outlined in Fig. 1.

The coating color-change response to the wall-jet shear field was recorded with a three-chip, co-site sampling, RGB video camera (SONY XC-007) linked to a frame grabber (MATROX IM-1280) and computer. The frame grabber was composed of an image processing board and a four-channel digitizer (one channel each for the red, green, and blue data signals plus a video synchronization signal) with eight bits of resolution per channel. Prior to imaging the color response, the measured RGB values were checked over all pixels to ensure proper exposure levels for the image.

For color measurements it is more useful to represent the signal in terms of hue, saturation, and intensity (HSI) rather than RGB. Hue is associated with the dominant wavelength in a mixture of light waves, saturation represents the dilution of a pure color by white light, and intensity relates to the brightness of the light.[12,13] Hue is the quantity of interest in color measurements, and because in the HSI system intensity is decoupled from hue, such color measurements are insensitive to small nonuniformities in illumination and to irregular signal gains across charge-coupled device (CCD) arrays. A real-time color space conversion from RGB to HSI was performed by the digitizer during image acquisition.

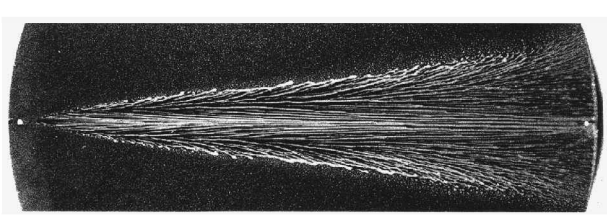

Fig. 3 Surface streakline pattern for $P_0 = 4$ psig.

The imaging system (illumination source, CCD camera, digitizer) was calibrated such that color measurements were referenced to a universal standard illuminant. The calibration reference was the Macbeth color checker,[14] which is a grid of 18 colors and 6 gray shades having known tristimulus values when illuminated by the Commission Internationale d'Eclairage illuminant C. Ten sequential images, approximately 100×100 pixels square, were captured of each color square of the Macbeth chart, and average tristimulus values were determined. A linear mapping was then calculated, which corrected the measured tristimulus values to their known reference values. The calibration procedure is fully detailed in Ref. 15 and was implemented here through the use of STANVIEW, a software package originally developed for liquid crystal thermography. This color calibration was applied to all subsequent measurements through a real-time lookup table on the digitizer board.

The uncertainty in LCC hue measurements was estimated by examining standard deviations of time records measured within a 4×4 pixel region located at the center of the test surface. One thousand images were recorded at 30 Hz for both the no-flow condition ($P_0 = 0$) and for flow at $P_0 = 4$ psig. The standard deviation of the hue, expressed as a percent of the time-averaged hue, was less than 0.6% at $P_0 = 0$ and less than 0.9% at $P_0 = 4$ psig for each of the time records corresponding to the 16 pixels of the imaged region. Clearly, this increase in hue uncertainty (flow vs no flow) was a direct result of fluctuations in the shear stress magnitude at the sampling point. The time constant of the LCC, however, has yet to be quantified, but the hot-film results suggest that the LCC does not follow the time scales of the local turbulence.

A second approach for estimating the measurement uncertainty was to examine variations of hue along the centerline core region of the jet-induced shear field where mean shear magnitude was spatially uniform. This approach is equivalent to a repeated single-measurement experiment, with each pixel treated as an individual sensor. The full test surface was imaged for flow at $P_0 = 4$ psig with the camera aligned with the jet axis ($\phi_C = \phi_J = 0$ deg). Five sequential images were time averaged, and statistics were calculated over a 3-pixel-wide by 44-pixel-long subregion along the jet centerline within the constant-shear core. Results yielded a standard deviation in hue of 1.0% of the mean value over this region, a value equivalent to the temporal standard deviation measured at a single pixel. This latter approach will be utilized in Sec. V to estimate measurement uncertainties for shear stress magnitude and vector orientation.

To measure the complete shear vector field, the LCC color-change response was imaged from seven different in-plane view angles ($\phi_C = 0, \pm 10, \pm 25$, and ± 45 deg) so as to encompass all possible shear vector directions. The camera above-plane view angle was held constant at $\alpha_C = 30$ deg. Flow was established, and five sequential images were then captured at the rate of 30 frames per second. Each image (584×286 pixels) of the complete test surface was color corrected and converted from RGB to HSI, and the resulting hue fields were time averaged. Examples of three cropped hue images, displayed in false colors that simulate actual liquid crystal color-change responses,[2] are shown in Fig. 4. Flow is left to right. The flow condition, $P_0 = 4$ psig, was the same as for the oil-flow visualization shown in Fig. 3. The images have been transformed to a common coordinate system, placing the images in register and removing perspective distortions caused by the oblique view angle α_C. The perspective coordinate system transformation (described later) was correct only for objects on the test surface; hence the jet nozzle and pitot tube appear distorted.

The $\phi_C = 0$ deg hue image is symmetric about the jet centerline due to camera alignment with the centerline shear vector direction and to the symmetry of the shear vector field itself (magnitudes and directions) relative to the centerline. The $\phi_C = \pm 45$ deg hue images are essentially mirror images, and each appears slightly asymmetric relative to the jet centerline. This asymmetry is a direct result of the

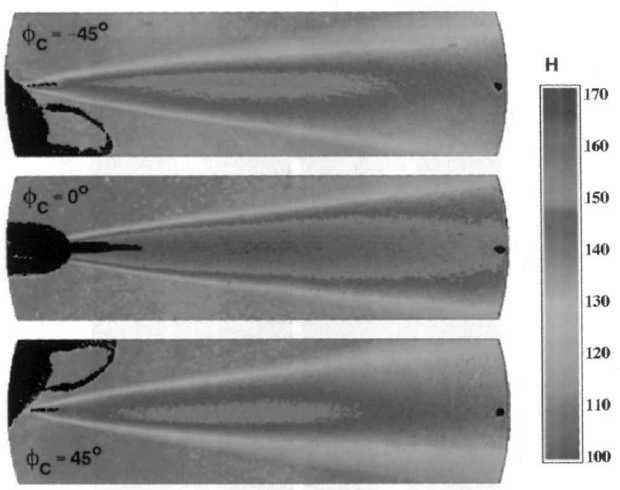

Fig. 4 Five-frame averages of measured hue for P_0 = 4 psig; images have been corrected for perspective and registered.

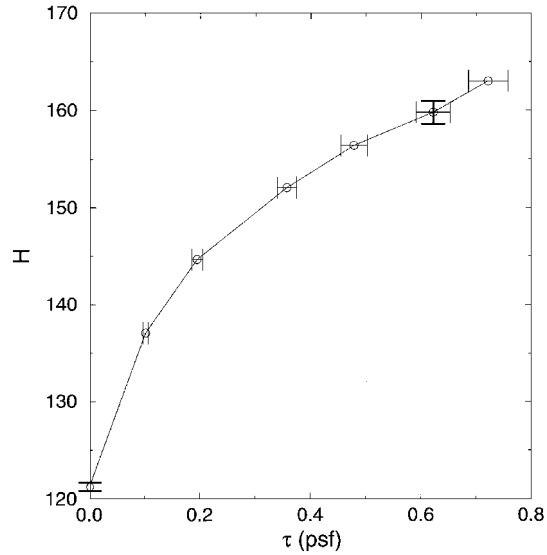

Fig. 5 Hue vs shear magnitude calibration for BCN/192; $\phi_C = \phi_\tau = 0$ deg.

dual dependence of coating color-change response on shear magnitude and shear direction relative to the observer; both quantities vary across the jet-induced shear field.

III. Shear Calibration

A variation of the fringe imaging skin friction (FISF),[8] or oil-drop, technique was used to calibrate and also to validate the liquid crystal measurement technique. The essence of the FISF method is that the mean shear magnitude at a point on a surface can be determined by measuring (post-test) the thickness of a drop of silicon oil after exposure to a steady flow for a known time period. Under shear, an oil drop deforms into an elongated thin layer with a well-defined leading edge and a linear thickness-vs-distance profile. An extended coherent light source oriented nearly perpendicular to the surface will create an interference pattern caused by the reflection of the light from the top surface of the oil interfering with the light reflected from the test surface. The distance between the interference bands is proportional to the thickness of the oil layer and, by lubrication theory, is proportional to the skin friction. If the resolution of the fringe imaging system and the visibility of the fringes are sufficient, the accuracy of the shear magnitude measurement is approximately $\pm 5\%$.

Using the FISF technique, shear stress magnitude at the center point of the disk ($x/D = 9$ and $y/D = 0$) was measured over a range of jet stagnation pressures, $0.5 \leq P_0 \leq 5.0$ psig. The color-change response of the LCC was measured vs jet stagnation pressure at the same point over the same P_0 range. For the LCC color measurements, the in-plane view angle of the camera was $\phi_C = 0$ deg and the above-plane camera angle was $\alpha_C = 30$ deg. Combining these results yielded the LCC hue-vs-shear magnitude calibration curve shown in Fig. 5. Statistics for hue were acquired only for the $P_0 = 0$ and 4 psig conditions, and corresponding standard deviations are indicated in Fig. 5. Uncertainties in the oil-drop shear magnitude measurements are shown as $\pm 5\%$ of each value.

IV. Image Processing and Analysis

Four image-processing and analysis steps were performed to determine the shear stress vector field from the measured color-change responses of the LCC. The first step, discussed earlier, was the real-time conversion of the measured RGB signals to hue.

The second step was an optional low-pass filter applied to the hue images. It was found that the spatial average over a 5×5 pixel neighborhood significantly reduced the local standard deviation of the hue, from 1.0 to 0.2% of the local mean, while preserving the hue gradients across the image. Results obtained both with and without application of this filter will be presented.

Third was a perspective coordinate system transformation that mapped the image coordinates to physical coordinates on the test surface and registered the images. This transformation was required because step 3 of the measurement methodology (see again Fig. 1) requires that the hue value for each in-plane view angle used in the curvefitting procedure be taken from the same physical location on the test surface.

This overall transformation is defined by the photogrammetric relations[12] and consists of two sequential transformations. The first removes perspective distortions and depends on the focal length of the imaging optics and on the geometry of the test surface. The second represents a three-dimensional coordinate system transformation between the system attached to the focal plane of the camera and the physical coordinate system attached to the test surface. Seven parameters are required to specify this transformation: three translations for camera position, three rotation angles for camera orientation, and the focal length of the optics. These parameters were determined for each image by solving the inverse transformation for the reference marks machined every 45 deg around the circumference of the test surface, i.e., solving for the parameters that map the known physical coordinates of the reference marks onto their respective images. The system of equations was solved iteratively with a convergence criterion that the mean difference between their actual and mapped locations, for all reference points used, be less than or equal to one pixel (0.01 in., in this case). This criterion resulted in image alignment to within ± 0.2 deg.

After mapping the images onto the physical coordinate system, the pixels no longer fall on a rectangular grid. A two-dimensional linear interpolation was thus performed to provide a rectangular grid of pixels at the finest resolution of the original image (0.01 in./pixel). Bicubic spline interpolation was also investigated; however, no measureable advantages were observed, whereas computation time increased manyfold compared with the linear interpolation.

The hue images shown in Fig. 4 are the results of the perspective coordinate system transformation and the interpolation, without the application of the low-pass filter. It should be noted that the interpolation procedure acted as a mild low-pass filter, reducing the local standard deviation of hue by about half.

The final analysis procedure was described earlier as step 3 of the measurement methodology. At each physical location on the test surface, the hue value corresponding to that location was taken from each ϕ_C image. Two example data sets of hue vs ϕ are shown in Fig. 6, one set taken from the jet centerline ($x/D = 9$ and $y/D = 0$) and the second set taken from the edge of the jet ($x/D = 9$ and $y/D = 0.9$). In the latter case, shear stress magnitude was near the lower limit of the calibrated range. A Gaussian curve was then fit to the hue vs ϕ data using a nonlinear least-squares method (the Levenburg–Marquardt method[16]). The angular location of the peak of the Gaussian curve gave ϕ_τ, the shear stress vector orientation as indicated on each curve of Fig. 6. The value of the hue at the peak of the Gaussian curve was then used in the hue vs τ calibration curve of Fig. 5 to determine the shear stress vector magnitude. The Gaussian

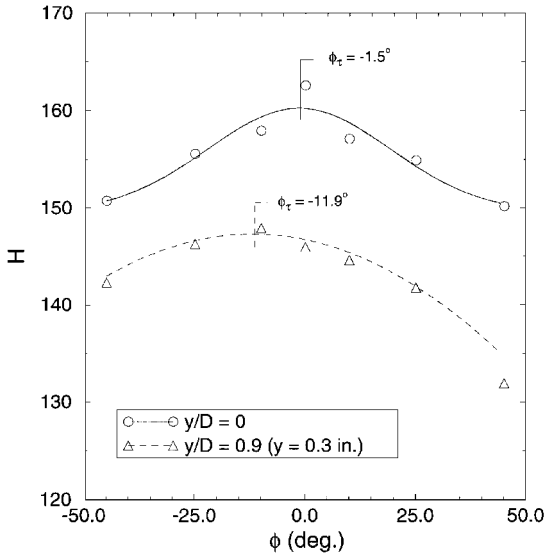

Fig. 6 Hue vs in-plane view angle at *x/D* = 9; data from seven images with Gaussian curvefits.

curvefit and the hue vs τ lookup were performed at every pixel in the image set to produce the full-surface shear stress vector field.

V. Results

Figure 7 shows two representations of the wall-jet-induced shear stress vector distribution as measured by the LCC technique. This data set was generated by analyzing seven low-pass-filtered hue images, and it contains approximately 10^5 measured vector values.

Both images shown in Fig. 7 use false color levels to represent the shear stress magnitude distributions. Vector orientations are illustrated by streaklines in Fig. 7a and by vector profiles in Fig. 7b. These streaklines, drawn tangent to the local shear stress vector at every point along their trajectories, were generated from the vector data set using the flow analysis software toolkit (FAST).[17] The vector profiles are drawn every $1.23D$ (every 40th profile) starting at the axial location of $x/D = 5$. For clarity, only every fourth vector is shown in each profile. Qualitatively, these results show a strong correlation to the combined features of the $\phi_C = 0$ deg hue image of Fig. 4 and the oil-flow pattern of Fig. 3, namely, a symmetric magnitude distribution and similar streakline patterns.

Quantitative comparisons with point measurements taken across the jet at a single axial station ($x/D = 9$) are shown in Fig. 8. The point measurements of magnitude were made using the FISF method as described in the section on shear calibration. Vector directions across this axial station were determined by measuring the tangent angle of the streaklines in the oil-flow visualization of Fig. 3. These comparisons show good overall agreement between the LCC measurements and the point measurements across the entire shear field. Note that the vector directions across the core region of the shear field ($-0.3 < y < 0.3$ in.) all fell between ± 10 deg and that the LCC technique measured these directions to within 1–2 deg even though no hue images were recorded between $\phi_C = 0$ and ± 10 deg. This is a clear indication of the robustness of the variation of hue vs ϕ and of the Gaussian curvefitting procedure used in the LCC methodology.

Uncertainty estimates for the LCC-defined shear magnitudes and vector orientations were determined by first examining the standard deviations of the data within the constant-shear core region of the jet-induced shear field. The statistics were calculated over a 3×20 pixel region centered about the $y = 0$ axis and having its long dimension aligned with the flow. This region covered a physical extent of 0.03×0.2 in., or $0.09D \times 0.6D$. Within this core region, the mean values and standard deviations were $\bar{\tau} = 0.61$ psf $\pm 6.2\%$ and $\bar{\phi}_\tau = -1.5 \pm 2.1$ deg, for the unfiltered data set, and $\bar{\tau} = 0.62$ psf $\pm 1.0\%$ and $\bar{\phi}_\tau = -1.9 \pm 0.3$ deg, for the low-pass-filtered data set. As expected, smoothing the original hue images resulted in less noise in the final shear stress vector field. Notice that the mean vector

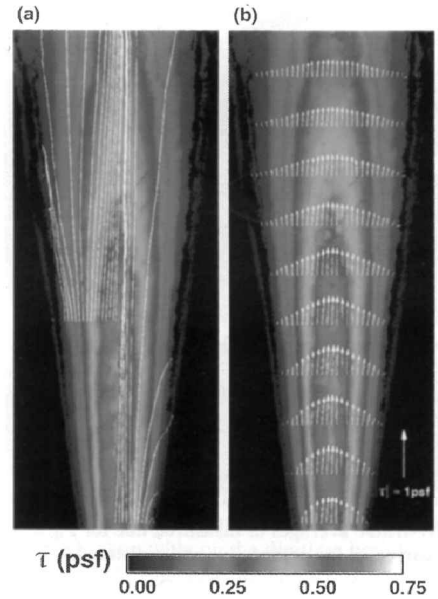

Fig. 7 Measured surface shear stress vector field for wall-jet flow at P_0 = 4 psig; color contours show vector magnitudes: a) vector orientations shown by streaklines originating from *x/D* = 5 and 10 and b) vector cross-stream profiles starting at *x/D* = 5 every Δ *x/D* = 1.23.

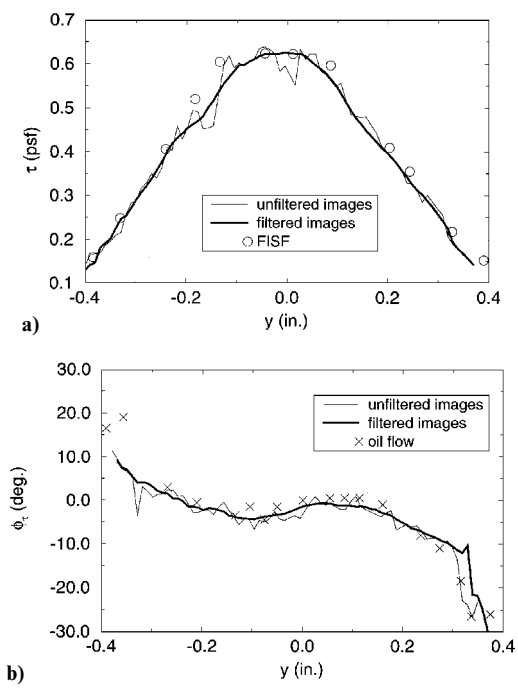

Fig. 8 Cross-stream profiles of wall-jet shear field at *x/D* = 9 for P_0 = 4 psig vs point measurements of magnitude and direction.

orientation was on the order of -2 deg, whereas an orientation of 0 deg was expected in this region due to the symmetry of the flow. Notice also that the 1–2 deg difference between LCC-measured and point-measured vector orientations (see Fig. 8b) was relatively constant across the central profile of the jet. Taken together, these facts indicate that the apparent skew of -1 to -2 deg in the mean orientation of the LCC measurements was most probably a result of limitations in aligning the jet tube axis with the principal diameter of the test surface. At best, this alignment was accurate to within 1 deg, estimated from flow visualization.

The procedure described earlier was also used to estimate LCC measurement uncertainties outside of the constant-shear core region, although a smaller, 3×9 pixel, sampling area was used. This area covered a physical extent of 0.03×0.09 in., or $0.09D \times 0.27D$. Figure 9 shows the standard deviation profiles for τ and ϕ_τ at the

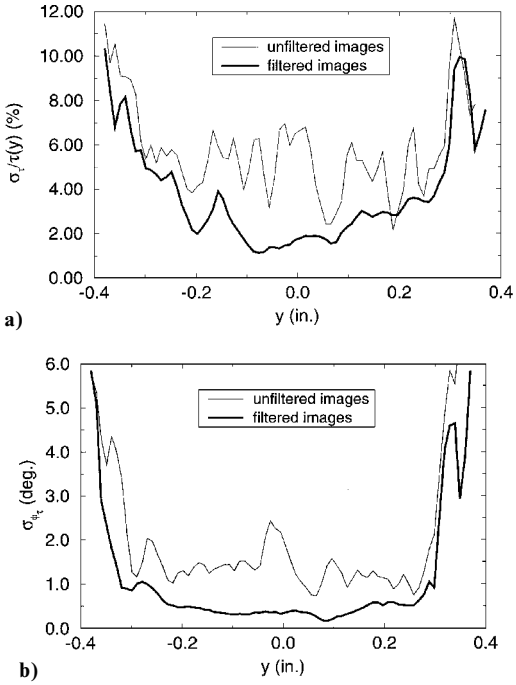

Fig. 9 Cross-stream profiles of measured standard deviations for results of Fig. 8: a) shear vector magnitude uncertainty, nondimensionalized by local shear magnitude (percent) and b) shear vector orientation uncertainty (deg).

$x/D = 9$ axial station. At each point along the cross-cut profile, the mean values and the standard deviations were calculated using the 3×9 pixel region centered around each point. Comparisons between the data values (τ and ϕ_τ) at each point and mean values showed that the shear field was sufficiently constant across this 3×9 pixel region for the standard deviations to reasonably estimate the measurement uncertainties. Furthermore, the statistics at $y = 0$ are consistent with those, quoted earlier, calculated using the 3×20 pixel region. This fact indicates that a sufficient number of samples have been used to estimate the standard deviation of the data.

Across the main extent of the shear field, $-0.3 < y < 0.3$ in., the standard deviations calculated from the unfiltered data were in the range of 4–6% of the local shear magnitude, with corresponding uncertainties of 1–2 deg in ϕ_τ. Standard deviations calculated from the filtered data sets were about half these levels, namely 2–4% of local shear magnitude and less than 1 deg in vector orientation.

At the edges of the shear field, for $|y| > 0.3$ in. ($|y/D| > 0.9$), the local shear magnitude decreases significantly, and the ability of the LCC technique to resolve vector orientations, and thus vector magnitudes, is degraded. In this low-shear limit, standard deviations of the orientation data were as high as 6 deg with corresponding shear magnitude uncertainties on the order of 10%.

This low-shear limitation is defined in the present methodology by four factors: 1) the low-shear response of the LCC mixture, 2) the resolution of the imaging system, 3) the total number of hue images acquired and the $\Delta\phi_C$ spacing between images, and 4) the analysis methods applied to these hue images.

Proper selection of LCC materials was discussed in Ref. 2. To measure a very wide range of shear magnitudes beneath a single flowfield, multiple experiments, incorporating first high and then low viscosity mixtures, may have to be performed. Imaging system resolution is governed by tradeoffs between accuracy requirements and cost.

Having more images with a smaller $\Delta\phi_C$ spacing between images may aid in localizing the peak in the hue vs ϕ data (recall Fig. 6); however, the tradeoffs here are an increase in analysis time and in required image data storage.

Finally, the analysis methods, particularly the Gaussian curve-fitting procedure, contribute to the low-shear sensitivity limit of the technique. To fit a Gaussian curve to hue vs ϕ data, a peak must be present in the data, there must be at least one datum to either side of this peak, and there must be a minimum of four data points. These criteria are difficult to satisfy as the magnitude of the shear vector approaches zero; in this limit, the shear-induced color change varies little from the no-shear background color, even for the optimum viewing orientation of $\phi_C = \phi_\tau$. Again, employing a higher-resolution imaging system and/or capturing more images at smaller $\Delta\phi_C$ spacings could help, to some extent, to satisfy these criteria. Employing smarter analysis techniques geared toward detecting peaks within noisy signals holds promise for improving the low-shear resolution of this technique.

Extension of this methodology to curved surfaces will require an understanding of the sensitivities of the observed color-change responses to variations in illumination angle and above-plane view angle, both measured relative to the local tangent plane at each surface point. A family of calibration curves (of hue vs shear magnitude), with camera above-plane view angle as the parameter, may be required to accomplish this next step.

VI. Conclusions

Based on present results, it has been shown that the liquid crystal coating technique can be utilized to obtain areal measurements of surface shear stress vector distributions on planar surfaces with accuracies equivalent to conventional point-measurement techniques.

This full-surface technique requires an image-based instrumentation system that incorporates white light illumination normal to the coated test surface and allows for oblique observations with an RGB color camera. Multiple in-plane view angles encompassing the shear vector directions to be measured are required while maintaining the same above-plane view angle ($\sim$30 deg) for each image.

The approach includes an illuminant-invariant color calibration procedure previously validated in research using thermochromic liquid crystal coatings for measurements of surface temperature distributions. A single calibration of color (hue) vs shear magnitude is required for the specific arrangement wherein the calibration shear vector is aligned with and directed away from the camera. Existing point-measurement techniques, such as oil-drop interferometry, can be utilized for this purpose.

Once color and shear calibrations have been accomplished, full-surface hue images are acquired as a function of in-plane view angle. For each physical point on the test surface, a Gaussian curve is fit to the hue vs in-plane view angle data. The in-plane view angle corresponding to the maximum hue value of the curvefit determines the vector orientation. This maximum hue value is then input to the hue vs shear magnitude calibration to determine the vector magnitude. This data analysis procedure is repeated for all surface points to determine the complete shear vector field.

Measurements of surface shear stress vector distributions beneath highly three-dimensional flows, including flows with regions of reversal, are now possible on planar surfaces, limited solely by optical access.

Acknowledgments

The STANVIEW software was transferred from Stanford University to NASA Ames Research Center royalty free under NASA Ames University Consortium Grant NCA2-807. The participation of Dino J. Farina of Stanford University in this research was made possible by this grant and a NASA Ames Graduate Student Researcher Fellowship. The authors gratefully acknowledge the software development support of R. K. McCabe and J. R. Lehman of the Data Analysis Branch at NASA Ames and K. C. Hu, D. J. Whitney, and D. G. Deardorff of Sterling Software Co. The participation of Michael C. Wilder of MCAT Inc. was made possible by NASA Contract NAS2-14109.

References

[1]Reda, D. C., Muratore, J. J., Jr., and Heineck, J. T., "Time and Flow Direction Responses of Shear-Stress-Sensitive Liquid Crystal Coatings," *AIAA Journal*, Vol. 32, No. 4, 1994, pp. 693–700.

[2]Reda, D. C., and Muratore, J. J., Jr., "Measurement of Surface Shear Stress Vectors Using Liquid Crystal Coatings," *AIAA Journal*, Vol. 32, No. 8, 1994, pp. 1576–1582.

[3]Fergason, J. L., "Liquid Crystals," *Scientific American*, Vol. 211, Aug. 1964, pp. 76–85.

[4]Klein, E. J., "Liquid Crystals in Aerodynamic Testing," *Astronautics and Aeronautics*, Vol. 6, July 1968, pp. 70–73.

[5]Hall, R. M., Obara, C. J., Carraway, D. L., Johnson, C. B., Wright, E. J., Covell, P. F., and Azzazy, M., "Comparisons of Boundary-Layer Transition Measurement Techniques at Supersonic Mach Numbers," *AIAA Journal*, Vol. 29, No. 6, 1991, pp. 865–871.

[6]Holmes, B. J., Gall, P. D., Croom, C. C., Manuel, G. S., and Kelliher, W. C., "A New Method for Laminar Boundary-Layer Transition Visualization in Flight: Color Changes in Liquid Crystal Coatings," NASA TM-87666, Jan. 1986.

[7]Haritonidis, J. H., "The Measurement of Wall Shear Stress," *Advances in Fluid Mechanic Measurements*, Springer–Verlag, New York, 1989, pp. 229–261.

[8]Zilliac, G., "Further Developments of the Fringe-Imaging Skin Friction Technique," NASA TM 110425, Dec. 1996.

[9]Reda, D. C., "Method for Determining Shear Direction Using Liquid Crystal Coatings," U.S. Patent 5,394,752, March 1995.

[10]Reda, D. C., "Method for Measuring Surface Shear Stress Magnitude and Direction Using Liquid Crystal Coatings," U.S. Patent 5,438,879, Aug. 1995.

[11]Reda, D. C., Wilder, M. C., and Crowder, J. P., "Simultaneous, Full-Surface Visualizations of Transition and Separation Using Liquid Crystal Coatings," *AIAA Journal*, Vol. 35, No. 4, 1997, pp. 615, 616.

[12]Gonzalez, R. C., and Woods, R. E., *Digital Image Processing*, Addison–Wesley, Reading, MA, 1992.

[13]Camci, C., Kim, K., and Hippensteele, S. A., "A New Hue Capturing Technique for the Quantitative Interpretation of Liquid Crystal Images Used in Convective Heat Transfer Studies," *Journal of Turbomachinery*, Vol. 114, No. 10, 1992, pp. 765–775.

[14]McCamy, C. S., Marcus, H., and Davidson, J. G., " A Color-Rendition Chart," *Journal of Applied Photographic Engineering*, Vol. 2, No. 3, 1976, pp. 95–99.

[15]Farina, D. J., Hacker, J. M., Moffat, R. J., and Eaton, J. K., "Illuminant Invariant Calibration of Thermochromic Liquid Crystals," *Experimental Thermal and Fluid Science*, Vol. 9, No. 1, 1994, pp. 1–12.

[16]Press, W. H., Teukolsky, S. A., Vetterling, W. T., and Flannery, B. P., *Numerical Recipes in C*, 2nd ed., Cambridge Univ. Press, Cambridge, England, UK, 1992.

[17]Bancroft, G. V., Merritt, F. J., Plessel, T. C., Kelaita, P. G., McCabe, R. K., and Globus, A., " FAST: A Multi-Processed Environment for Visualization of Computational Fluid Dynamics," *Proceedings, IEEE Visualization '90 Conference* (San Francisco, CA), Inst. of Electrical and Electronics Engineers, 1990, pp. 14–24.

G. Laufer
Associate Editor

Color reproduction courtesy of NASA Ames Research Center